Supporting information

Photoelectric Memristor Based on PZT/NSTO Heterojunction for Neuromorphic Computing applications

Jingjuan Wang,[2] Zhaowen Wang,[1] Wenze Zhao,[1] Xiaobing Yan[1,3]*

[1]National-Local Joint Engineering Laboratory of New Energy Photovoltaic Devices, Key Laboratory of Brain-Like Neuromorphic Devices and Systems of Hebei Province, College of Electron and Information Engineering, Hebei University, Baoding, 071002, China

[2]Hebei Key Laboratory of Optoelectronic Information and Geo-detection Technology，School of Information Engineering, Hebei GEO University, Shijiazhuang, 050031, China

[3]Department of Materials Science and Engineering, National University of Singapore, Singapore 117576, Singapore

**Correspondence should be addressed to X.B.Y. (email: yanxiaobing@ime.ac.cn)*

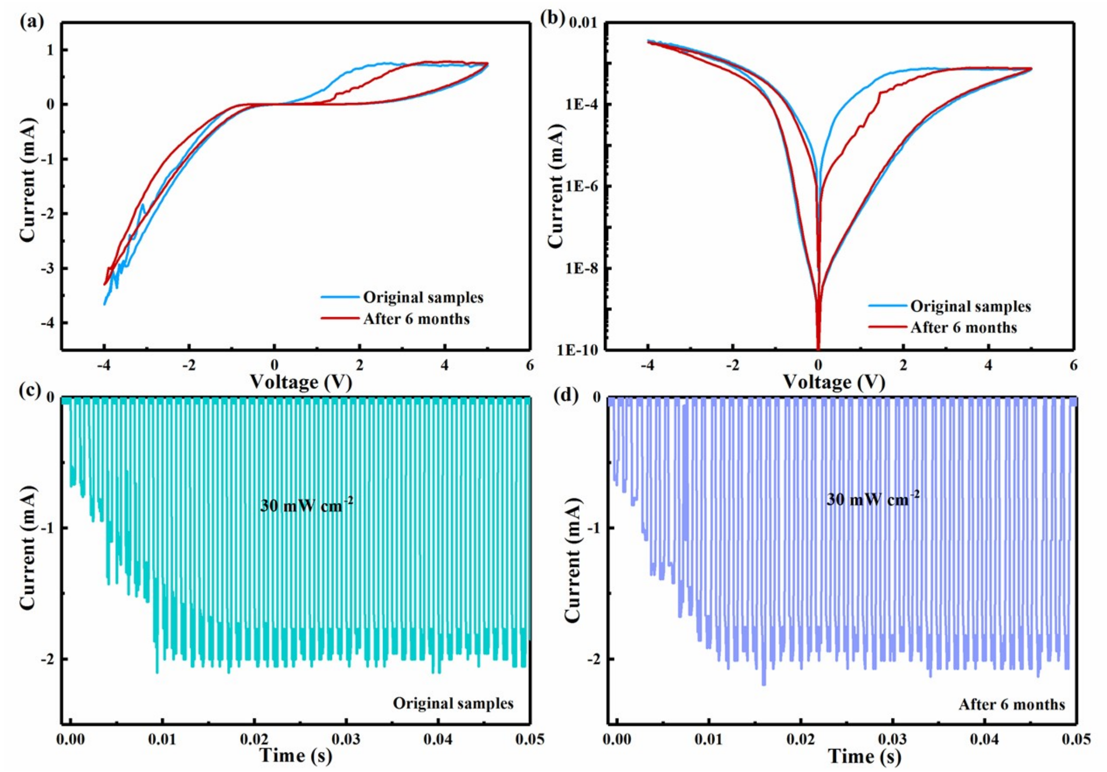

Fig. S1. The device-to-device uniformity of synapses. (a)-(b) The I-V curves of Pd/PZT/NSTO devices. (c) The EPSC graph of original Pd/PZT/NSTO optical synaptic device for sequential light pulses with 2KHz frequency and (e) the same measurements after 6 months for the another similar device.

Fig. S2. Endurance characteristics

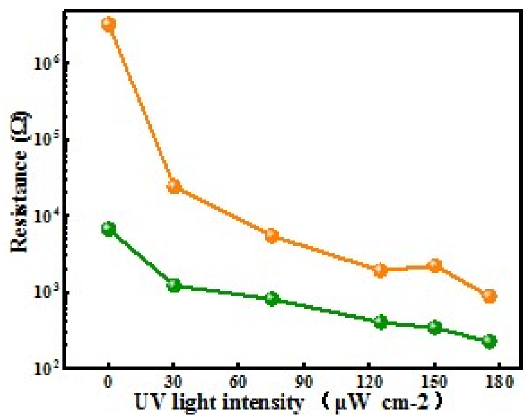

Fig. S3. Comparisons of HRS and LRS data with different power densities.

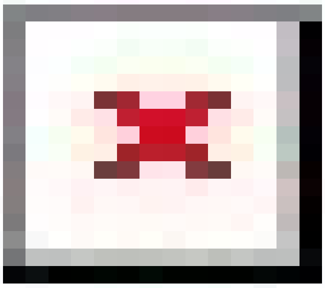

Fig. S4. The absorbance spectra of PZT/NSTO heterojunction memristor

The built-in electric field in PZT/NSTO heterostructure and its influence on ferroelectric polarization and resistance switching behavior can be explained by the energy band structure of PZT/NSTO heterostructure. Fig. S4a shows the structural diagram of Pd/PZT/NSTO device. After applying a positive electric field, the ferroelectric polarization in PZT film is upward (p_{up}). If we regard PZT and NSTO as broadband gap semiconductors without considering the polarization charge, the energy band structure of PZT/NSTO heterostructure can be shown in Fig. S4b. For NSTO, the electron affinity and band gap were 4.0 and 3.2 eV, respectively. In the NSTO substrate with high conductivity, it is an n-type semiconductor with a work function of 4.2 eV due to Nb substitution doping (i.e., Nb^{5+} substitution for Ti^{4+} positions).[1,2] For PZT, the electron affinity and band gap are 3.5 eV and 3.4 eV, respectively. According to many research results, PZT should be a p-type semiconductor due to the loss of oxygen. Therefore, its Fermi level is low but close to the middle of the energy band gap, and its work function is 5.8 eV. [3,4] Due to different work functions, the energy band bends at the PZT/NSTO interface. Therefore, an induced built-in electric field (E_{bi}) pointing from NSTO to PZT is formed on the interface, which is similar to the semiconductor p-n junction, and a depletion layer is formed in the PZT layer near the PZT/NSTO interface. However, PZT is not only a p-type semiconductor, but also a ferroelectric semiconductor. If we consider the ferroelectric polarization of PZT films, the above situation will be changed. After applying a negative electric field, when the ferroelectric polarization of PZT layer is down, a positive polarization charge appears in the PZT/NSTO interface region. Therefore, most carriers in NSTO will be attracted to the PZT/NSTO interface region by positively polarized charges, so the width of built-in electric field (E_{bi}) and loss layer will be reduced, as shown in Fig. S4c. This condition corresponds to LRS in resistance switching behavior. On the contrary, after the positive electric field is applied, when the iron is polarized upward (p_{up}), the negative polarization charge accumulates in the PZT/NSTO interface region. Therefore, most carriers in NSTO are repelled by negative polarization charges and migrate to the interface region. Therefore, the width of built-in electric field (E_{bi}) and loss layer increases, as shown in Fig. S4d. This condition corresponds to HRS in resistance switching behavior In addition, although the magnitude of the built-in electric field can be strongly modulated under the action of ferroelectric polarization, the direction of the built-in electric field remains unchanged. Therefore, it can be considered that the modulation effect of ferroelectric polarization on the width of loss layer (Fig. S4c and S4d) leads to two states of LRS and HRS in resistance switching behavior. On the other hand, as mentioned above, there is an interface electric field similar to p-n junction on the PZT/NSTO interface. The direction of the interface electric field is always from NSTO to PZT, resulting in the formation of a hard switchable domain in the PZT layer near the PZT/NSTO interface. Therefore, since the interface domain tends to P_{up} rather than P_{down}, the hysteresis loop will show asymmetry.

It has been reported that the oxygen vacancy concentration at the interface of ferroelectric electrode can adjust the electrical properties, and the oxygen vacancy aggregation at the interface can reduce the barrier height at the interface and produce more current.[5,6] When PZT film absorbs photon energy under UV irradiation, it will produce electron hole pairs, and UV can enhance the mobility of charged substances and attract them from the interior of ionic crystals to the surface.[7] Therefore, under UV irradiation, it can promote the accumulation of oxygen vacancies on PZT/NSTO interface and increase the concentration of oxygen vacancies on the interface, Thus, the effective built-in electric field and depletion layer width of PZT/NSTO interface are reduced as shown in Fig. S4f, so more photocurrent can be realized.

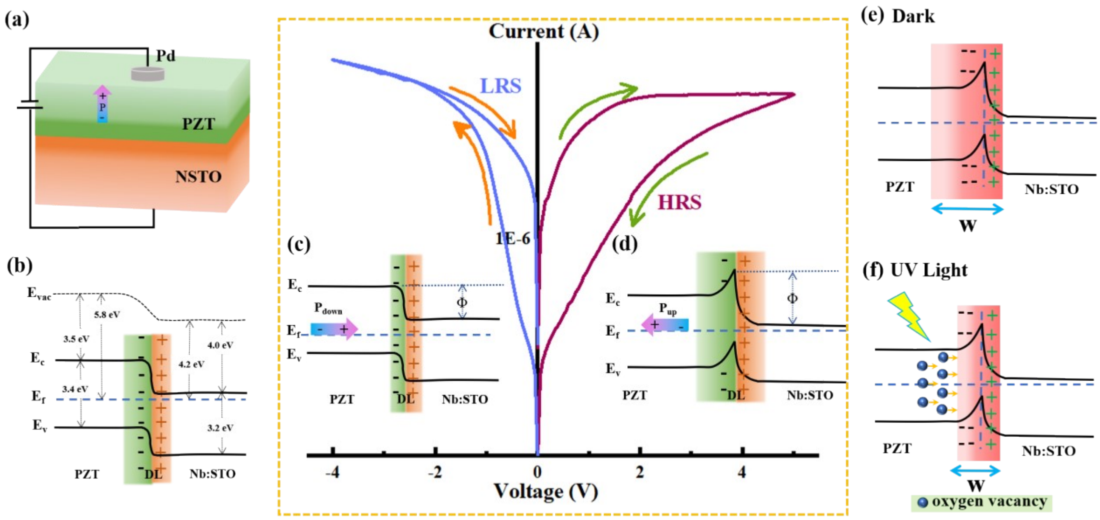

Fig. S5. (a) Schematic of the Pt/PZT/NSTO heterostructure under an applied electric field (DL represents "depletion layer"). (b-d) Band structure diagrams for the PZT/NSTO heterostructure in the different states: (b) in the state without considering the polarization, (c) in the state of polarization downward (LRS), and (d) in the state of polarization upward (HRS).

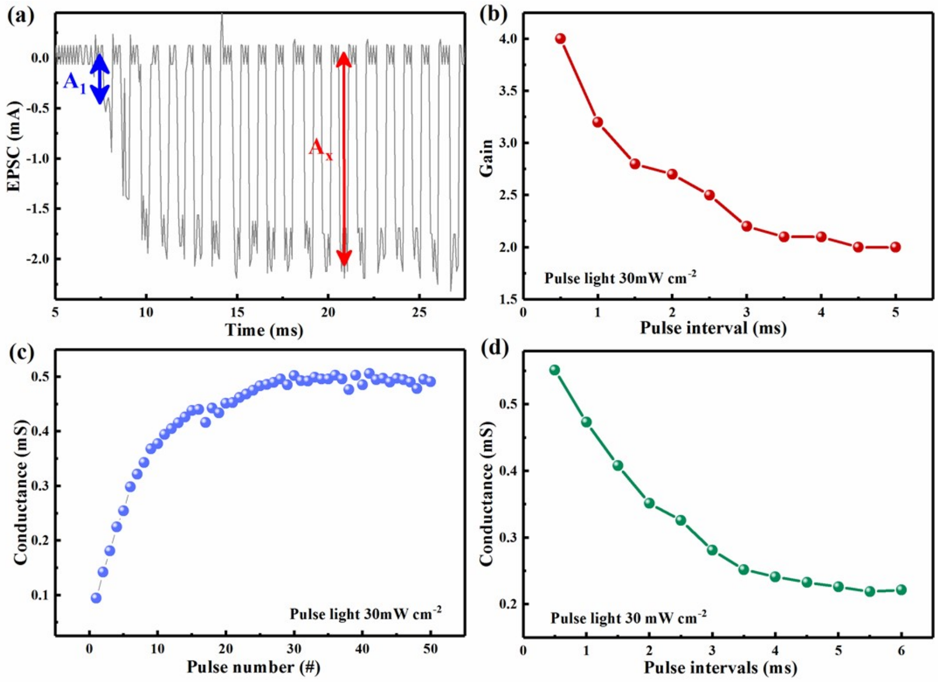

Fig. S6. (a) Gain is defined as the ratio of A_x /A_1. Here the twentieth peak was chosen as the representative of A_x. (b) The impact of pulse intervals on the gain characteristic s of devices. (c)-(d) The impact of pulse number and pulse interval on conductance of optical synapses.

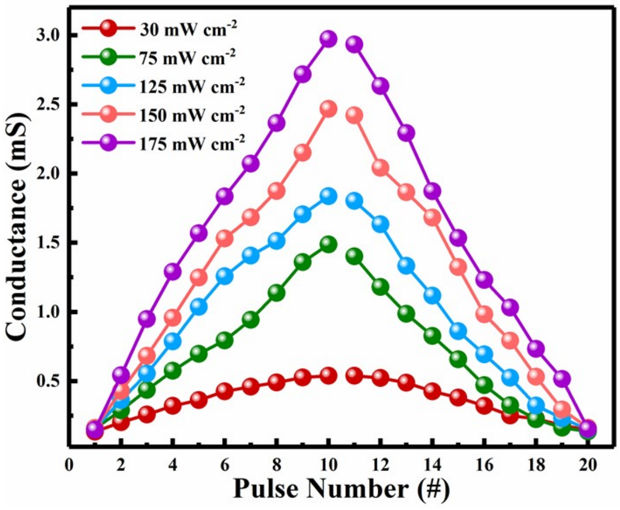

Fig. S7. The conductance variation under different light intensities when the device was programmed by a series of 10 identical negative pulses (-3 V, 0.5 ms) followed by a series of 10 identical positive pulses (+5 V, 0.5 ms).

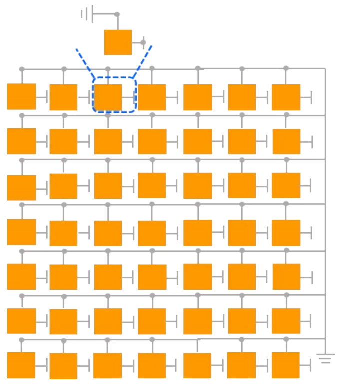

Fig. S8. Readout circuit of the photonic artificial synapse in the 7×7 array.

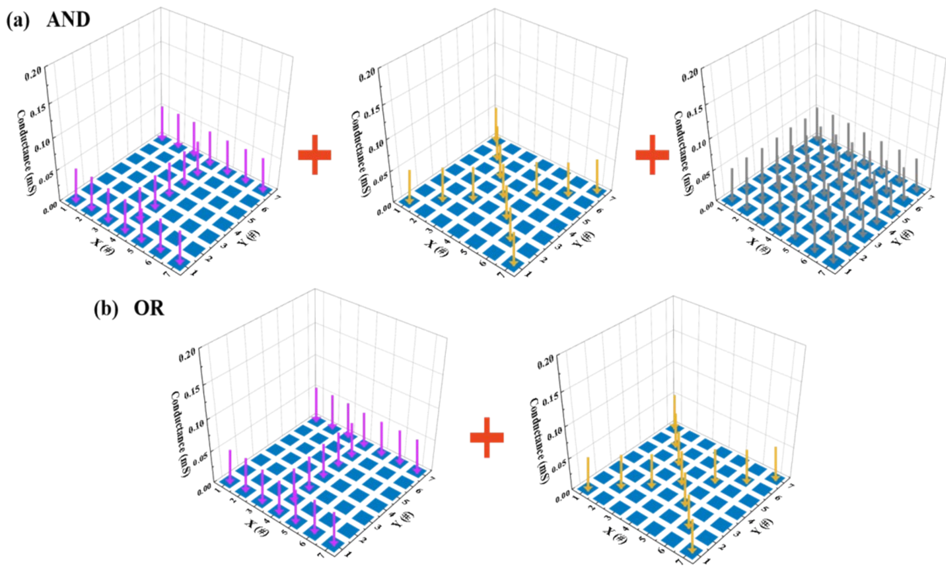

Fig. S9. (a) The light pulses, negative voltage pulses and positive voltage pulses were applied to memristors array for the realization of logic “AND”. (b) The light pulses and negative voltage pulses were applied to memristors array at the same time to realize logic “OR” operation.

There is an interfacial electric field existing at the PZT/NSTO interface like the p-n junction (**Fig. S10**). The direction of the interfacial electric field is always from NSTO to PZT, leading to that the hard switchable domains form at the PZT/NSTO interface. Therefore, the hysteresis loops are asymmetric because the interfacial domains tend to P_{up} rather than P_{down}. Moreover, in a thicker PZT film, the width of depletion layer will take a smaller proportion relative to the thickness of the PZT film, thus the effect of the ferroelectric domains inside the depletion layer on the total ferroelectric polarization switching will be weakened.

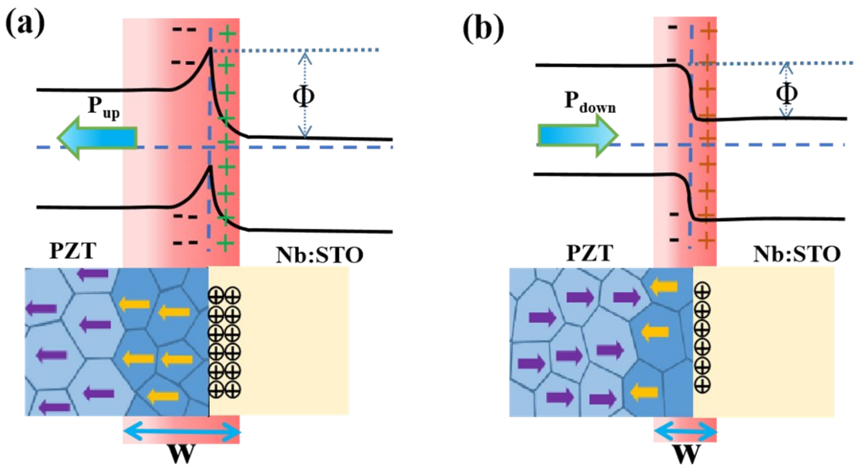

Fig. S10. Schematic diagrams of domain pinning at (a) P_{up}, and (b) P_{down} state.

The ferroelectricity of the device becomes better with the increase of thickness ,as shown in Fig. S4a-c. Fig. S4d-f shows that the thinner the thickness of PZT film, the leakage of I-V will occur.

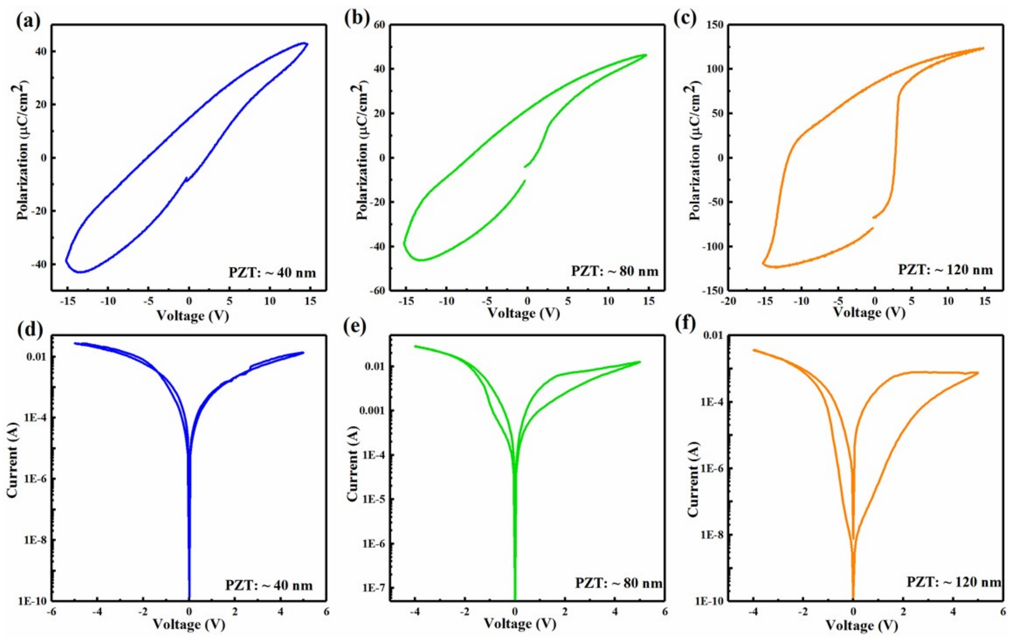

Fig. S11. (a) -(c) P−V characteristics of the PZT films with different thicknesses (40nm, 80nm, 120nm). (d)-(f) I-V characteristics of the PZT films with different thicknesses (40nm, 80nm, 120nm).

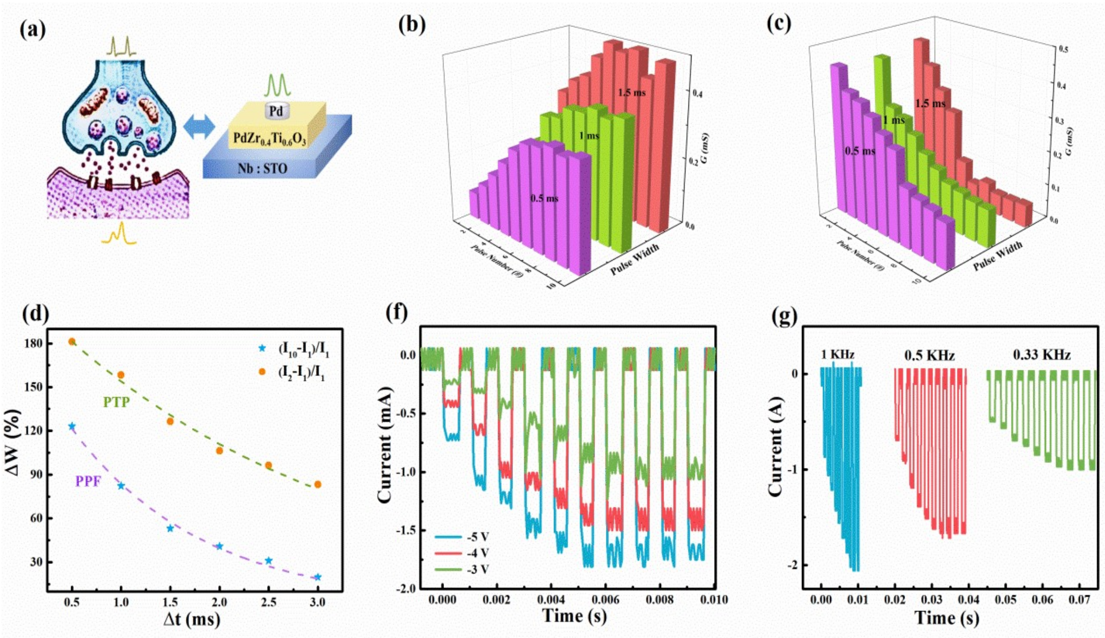

Fig. S12. (a) Schematic illustration of biological synapse and its analogue artificial synapse. Presynaptic pulses correspond to electrical stimuli. (b) The change of EPSC under different pulse number and pulse width. (c) The change of IPSC under different pulse number and pulse width. (d) Extracted PPF and PTP index versus impulse interval Δt, where I_1, I_2, and I_{10} are the recorded current after the first. (e) Current dependence recorded during the applying of ten stimulation pulses with different pulse amplitudes (-3, -4, and -5 V). (f) Current responses to ten identical stimulation pulses (V_{pos} = -5 V) at different frequencies (1.25, 0.59, and 0.38 Hz)

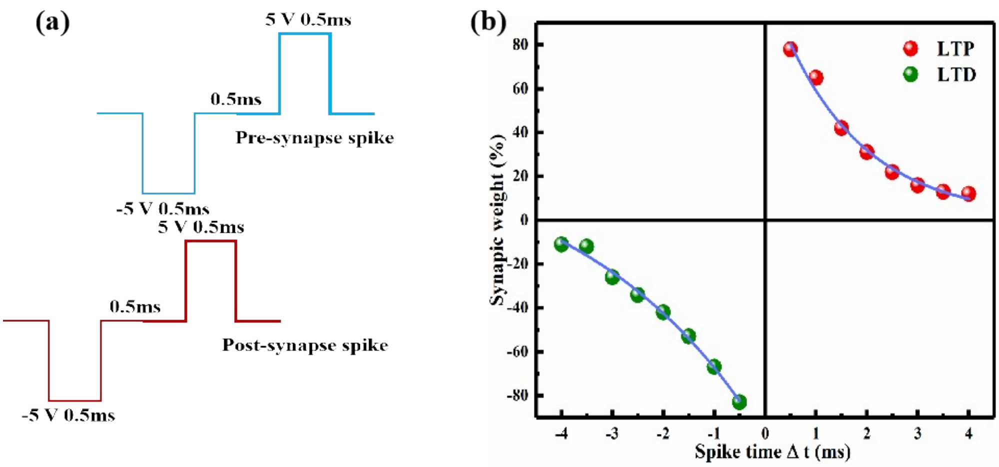

Fig. S13. The STDP perfomence of the memristor.

Table S1. Comparison of previously reported heterojunction memristor with this work.

Materials	**Availability of stimuli**	**Endurance Cycles**	**Intensity (mW/cm^2)**	**Light-induced synaptic plasticity**	**Application**	**Ref**
CeO_{2-x}/AlO_y	Electric+Optical	—	2.1-12	No	Boolean logic	8
CeO_2/MoS_2	Electric+Optical	—	0-10.842	EPSC/PPF/PPD STM /LTM	Color recognition/pain sensing capability	9
CeO_2/Nb−$SrTiO_3$	Electric	200	No	No	identify the electrocardiogra m (ECG) data	10
Ga_2O_3/MoS_2	Electric+Optical	—	0.391-3.290	EPSC/PPF/ STM /LTM	perception-memory integrated human visual system	11
Ga2O3/ Nb:SrTiO3	Electric	—	No	No	handwritten picture data	12
ZnO/Chl-A/Chl-D	Electric+Optical	—	1.1-80.2	IPSC/EPSC/PPF/ PPD STM /LTM	edge detection	13
Pyr-GDY/Gr/PbS-QD	Electric+Optical	—	150/10	PPF, SRDP		14
WO3/WSe2	Electric+Optical	—	—	STP/STD/PPFST P/STD	—	15
MoSe2/Bi2Se	Electric+Optical	1000	—	PPF	Image recognition/ Artificial retinal prostheses	16
POx/BP	Electric+Optical	—	—	STP/LTP/PPF	Pavlov's dog experiment	17
ZnO/PbS	Electric+Optical	—	0.7/800	EPSC/IPSC/PPF /PPD	distinguish the letter images	18
$CsPbBr_3$QDs /IGZO	Electric+Optical	400	12/16	EPSC/STM/LTM	Pavlov's dog experiment	19
$TiNxO_{2-x}$ /MoS_2	Electric+Optical	300	3.58	EPSC/PPF/ STM/ LTM	Image mapping	20
ZnO/PVSK/InO_x /Li-AlO_x	Electric+Optical	—	Bright/625 /525 /465	EPSC/PPF	cascaded near-sensor face recognition	21
PZT/NSTO	Electric+Optical	4000	30/75/125/150/ 175	EPSC/STP/LTP	Tetris game/Boolean logic computing	This work

Reference

1 H. M. Yang, L. H., Luo, H. M., Wang, H., Usov, I. O., Suvorova, N. A., Jain, M., D. M. Feldmann, P. C. Dowden, R. F. Dowden, Q. X. Jia, Appl. Phys. Lett. 2008, 92, 102113.

2 L. Zhao, Z. Lu, F. Zhang, G.Tian, X. Song, Z. Li, K. R. Huang, Z. Zhang, M. H. Qin, S. J. Wu, X. B. Lu, M. Zeng, X. S. Gao, J. Y. Dai, Liu, J. M. Sci Rep-UK, 2015, 5, 1-6,

3M. G. Han, M. S. Marshall, L.Wu, M. A.Schofield, T. Aoki, R. Twesten, J. Hoffman, F. J. Walker, C. H. Ahn, Y. Zhu, Nat. Commun. 2014, 5, 1-9.

4 J. Robertson, Measurement, J. Vac. Sci. Technol. B. 2000, 18, 1785-1791.

5 B. Nagaraj, S. Aggarwal, T. K. Song, T. Sawhney, R.Ramesh, Phys. Rev. B, 1999, 59, 16022.

6 R. Schafranek, S. Payan, M. Maglione, A. Klein, Phys. Rev. B. 2008, 77, 195310.

7 J. H. Booske, R. F. Cooper, S. A. Freeman, K. I. Rybakov, V. E. Semenov, Phys. Plasmas. 1998, 5, 1664-1670.

8 H. Tan, G. Liu, H. Yang, X. Yi, L. Pan, J. Shang, S. Long, M. Liu, Y. Wu, R.-W. Li,ACS Nano. 2017, 11, 11298-11305.

9 Y., Lin, W.,Wang, R., Li, J., Kim, C., Zhang, H., Kan, &Y. Li, Nano Energy, 2024,121, 109267.

10 H. Li, S. Geng, T. Liu, M. Cao, J. Su, ACS Appl. Mater. Interfaces. 2023, 15, 5456-5465.

11 LR., i, W., Wang, Y., Li, S., Gao, W., Yue, & SG. hen, Nano Energy, 2023, 111, 108398.

12 Y., Wang, W., Hu, K., Kang, DC., ong, & X. Tang, J. Phys. Chem. Lett. 2024,15, 11182-11188.

13 J., Jiang, X., Shan, J., Xu, Y., Sun, T. F., Xiang, A., Li, X. F. Wang, Adv. Funct. Mater. 2024, 2409677.

14 Y.-X. Hou, Y. Li, Z.-C. Zhang, J.-Q. Li, D.-H. Qi, X.-D. Chen, J.-J. Wang, B.-W. Yao, M.-X. Yu, T.-B. Lu, J. Zhang, ACS Nano, 2021, 15, 1497 – 1508.

15 H. K., He, R., Yang, H. M., Huang, F. F., Yang, Y. Z., Wu, J., Shaibo, & X. Guo, Nanoscale, 2020, 12, 380-387.

16 Y., Wang, J., Yang, Z., Wang, J., Chen, Q., Yang, Z., Lv, S. T. Han, Small, 2019, 15, 1805431.

17 S., Lee, R., Peng, C., Wu, & M. Li, Nat. Commun. 2020, 13, 1485.

18 H. Li, X. Jiang, W. Ye, H. Zhang, L. Zhou, F. Zhang, D. She, Y. Zhou, S.-T. Han, Nano Energy, 2019, 65, 104000.

19 S. Subramanian Periyal, M. Jagadeeswararao, S.E. Ng, R.A. John, N. Mathews, Adv. Mater. Technol. 2020, 5, 2000514.

20 W. Wang, S. Gao, Y. Li, W. Yue, H. Kan, C. Zhang, Z. Lou, L. Wang, G. Shen, Adv. Funct. Mater. 2021, 31, 2101201.

21 Q. Liu, L. Yin, C. Zhao, J. Wang, Z. Wu, H. Lei, Y. Liu, B. Tian, Z. Zhang, Z. Zhao, R. Liu, C. Ding, Y. Han, C.-Q. Ma, P. Song, I.Z. Mitrovic, E.G. Lim, Z. Wen, Nano Energy. 2022, 102 , 107686.